energies

MDPI

Article

Impact of a Connection Structure of Macro Fiber Composite Patches on Energy Storage in Piezoelectric Energy Harvesting from a Rotating Shaft

Piotr Micek and Dariusz Grzybek *

Faculty of Mechanical Engineering and Robotics, AGH University of Science and Technology, al. Mickiewicza 30, 30-059 Kraków, Poland

* Correspondence: dariusz.grzybek@agh.edu.pl; Tel.: +48-126-173-080

Abstract: Energy collection in a capacitor, which was charged by four connection structures of Macro Fiber Composite (MFC) patches, was the subject of laboratory research. The first structure was the delta circuit created by three MFC patches and connected with a three-phase rectifier; the second structure was the delta circuit created by three MFC patches and connected with a three-phase rectifier; the third structure was the parallel connection of three circuits, each of which consisted of an MFC patch and a full bridge rectifier; and the fourth structure the series connection of three circuits, each of which consisted of an MFC patch and a full bridge rectifier. Laboratory experiments were carried out on a laboratory stand which consisted of a rotating shaft, three MFC patches powering an energy storage system, and a data acquisition system. The star connection generated the highest values of voltage across a capacitor in the long time period. The delta connection produced the highest capacitor-charging power. The shortest time to reach a target voltage on the capacitor equal to a few volts was achieved by use of the delta or parallel connection. The delta connection generated target voltage equal to a few volts across a capacitor in the shortest time at a lower level of stress in the shaft, but the difference between the charging times by the delta circuit and by the parallel connection decreased as the stress in the shaft increased.

Keywords: piezoelectric energy harvesting; rotational piezoelectric energy harvesting; piezoelectric harvester; Macro Fiber Composite; energy storage; machine shaft

Citation: Micek, P.; Grzybek, D. Impact of a Connection Structure of Macro Fiber Composite Patches on Energy Storage in Piezoelectric Energy Harvesting from a Rotating Shaft. *Energies* **2022**, *15*, 6254. https://doi.org/10.3390/en15176254

Academic Editor: Philippe Leclère

Received: 21 July 2022
Accepted: 22 August 2022
Published: 27 August 2022

1. Introduction

Mechanical energy can be converted into electrical energy by the use of piezoelectric materials: ceramics, polymers, or composites. The energy conversion that takes place in the piezoelectric material is the result of stress generation in this material under the acting impact of a source of mechanical energy. Generating stresses in a piezoelectric material usually requires the use of additional mechanical elements, which are most often a cantilever beam or membrane. A structure that contains piezoelectric material and such additional mechanical elements is called a piezoelectric harvester in the literature.

Rotary elements, e.g., fans [1], car wheels [2], platforms [3], or machine shafts [4] are examples of source of mechanical energy in the scientific research on energy harvesting. Rotating sources of mechanical energy are usually used to generate motion of additional mechanical elements of the harvester, which is most often vibration of the cantilever beam [5]. The use of a cantilever beam in rotational piezoelectric harvesting may differ in three main areas: the location of the beam fixing, the ways in which the beam is forced to vibrate, and the longitudinal section of the beam. The cantilever beam may be fixed to a rotating element, e.g., [6], or to a motionless element which is located outside the rotating element, e.g., [7]. The vibrations of the cantilever beam may be induced by mechanically connecting the rotating element to the fixing of the cantilever beam, e.g., [8], or without contact by using, e.g., magnets [9]. The cantilever beam usually has a rectangular

longitudinal cross-section, e.g., [10]; beams with other shapes, e.g., triangular [11], are tested less frequently. In the articles cited above, piezoelectric energy harvesting is based on the kinematic forcing of the cantilever beam, which is part of the mechanical structure of the harvester. Piezoelectric energy harvesting can also be realized by directly transferring stresses that occur in a rotating element to a piezoelectric material. The basic condition for the effectiveness of such a process of energy harvesting is the occurrence of changeable stresses in the rotating element. Loaded machine shafts can be a source of mechanical energy in such an energy-harvesting process [12]. It should be noted that direct gluing of the piezoelectric material on the machine shaft prevents parametric optimization of the harvester mechanical structure, which is possible in piezoelectric energy harvesting from, e.g., from mechanical vibration [13].

Energy harvesting from a rotating element can be realized by using a single piezoelectric element [1–12] or bigger numbers, e.g., two [14], three [15], four [16], six [17], eight [18], nine [19], or twelve [20]. If one piezoelectric element is used, it is connected directly to one full bridge rectifier, which is a main element of the electric part of harvester. Standard energy harvesting (SEH) [21], extended versions of SEH (e.g., [22]), synchronized switch harvesting on inductor (SSHI) or extended versions of SSHI (e.g., [23]), are used as the electrical part of a harvester. If several piezoelectric elements are used, each of these items can be equipped with the same rectifier (e.g., SEH) or all of these piezoelectric elements can be connected to one rectifier. Any number of piezoelectrics can be connected in parallel [14,24] or in series [25] regardless of the voltage waveforms generated by these piezoelectrics only in applications where each piezoelectric is connected to a separate full bridge rectifier.

Any number of piezoelectrics can be connected to each other in parallel or in series to one full bridge rectifier in SEH only when the voltage waveforms generated by these piezoelectrics are the same or opposite [16]. Kurt et al. [26] and Bouzelata et al. [27] proposed connecting three piezoelectric beams, each of which generates a different voltage waveform, to one three-phase rectifier circuit using a star connection. Micek et al. [15] compared electric responses (voltage and power) in the process of energy harvesting with a three-phase rectifier, for both star and delta connections, with electric responses in the process of energy harvesting which uses parallel and serial connections of three circuits consisting of an MFC patch and a full bridge rectifier. They found that delta energy generation led to the greatest electrical power generation compared to any other connection.

It should be noted that the cited scientists [15,26,27] focused on examination of the aforementioned energy-harvesting systems with a three-phase rectifier for a resistive load. The results of the research on electric energy storage for the aforementioned energy-harvesting systems with a three-phase rectifier have not been presented in the literature so far. Taking into account that the harvested electric energy is usually not be enough to permanent power supply to any receiver, research on energy storage in the aforementioned energy-harvesting systems with a three-phase rectifier should be conducted. So, a research question arises: how will the use of a three-phase rectifier affect the energy storage process? In order to find an answer to this question, the authors of this article conducted experimental studies of four connection structures of three Macro Fiber Composite (MFC) patches with a rectifying system. The MFC patches were glued every 120 degrees to the surface of the shaft, which was cyclically bent. MFCs generate sinusoidal voltage waveforms also shifted by 120 degrees. Therefore, they cannot be connected in series or in parallel before rectifying the voltage, because the voltage values will partially cancel out. So, full bridge rectifiers and a series or parallel connection after rectifying the voltage were used (often used in the literature e.g., [14,25]). It was noticed that the sinusoidal waveforms generated by the MFC are shifted by 120 degrees, which corresponds to three-phase AC systems. A delta or star connection is commonly used in electrical engineering to connect such three-phase voltages e.g., in [28]. Therefore, the article also examined such two-connection structures. The authors presented the results of experimental studies of these structures for a resistive load in their previous article [15]. This article presents the results of experimental studies for a capacitive load. It was assumed that the energy would be stored in a capacitor,

which is used in the experiments of other researchers in the field of piezoelectric energy harvesting [29,30]. The state of the art is extended by describing the impact of the application of energy-harvesting systems (delta and star) with a three-phase rectifier on an energy storage process in the capacitor, which is charged by these energy-harvesting systems.

2. Research Methods

2.1. Structure of Laboratory Stand

Laboratory experiments were carried out on a laboratory stand which consisted of three main parts: a rotating shaft equipped with a rotational-motion-setting system and a load-setting system, three MFC patches powering an energy storage system, and a measurement system. The schema, which presents connections among these parts, is shown in Figure 1.

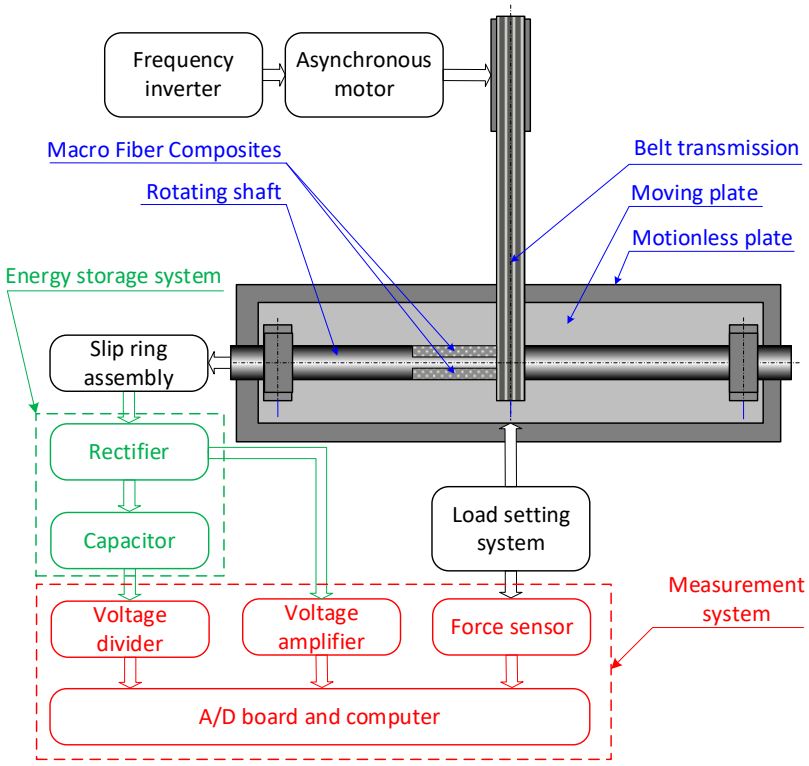

Figure 1. Schema of laboratory stand.

The rotating shaft, fixed in two bearings, was made from steel and had an annulus cross-section. Dimensions and material constants of the rotating shaft are listed in Table 1.

Table 1. Dimensions and material constants of shaft [15].

Parameter	Symbol	Unit	Value
External diameter of shaft	Dso	mm	40
Internal diameter of shaft	Dsi	mm	36
Young's modulus of steel	Ys	Pa	205×10^9
Distance between bearing and center of shaft	1_1	mm	310
Distance between bearing and center of shaft	1_2	mm	310

The rotational-motion-setting system consisted of a belt transmission and an asynchronous motor equipped with a frequency inverter. The rotational speed of the motor, which drove the belt transmission, was controlled by the frequency inverter. The belt transmission generated a rotational speed of the shaft in a range from 1 to 20 rps. The

load-setting system consisted of a screw gear mechanism, which caused changes in the values of the force acting on the shaft. Screwing in or screwing out caused an increase or decrease in this force. This system generated force, which acted on shaft, in a range from 0 to 1000 N.

The view of the mechanical parts, which were mounted in the laboratory stand, is presented in Figure 2.

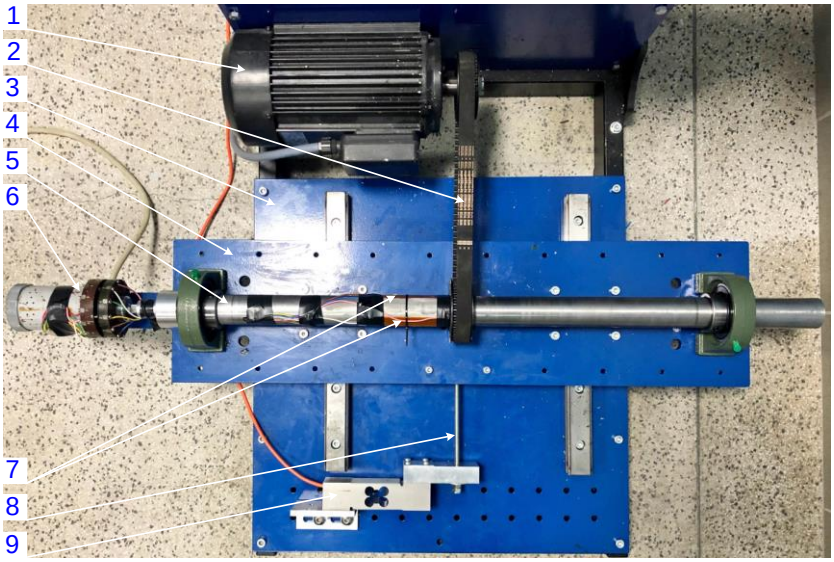

Figure 2. View of the structure of laboratory stand [15]: 1—asynchronous motor, 2—belt transmission, 3—motionless plate, 4—moving plate, 5—rotating shaft, 6—slip ring assembly, 7—patches of Macro Fiber Composite, 8—screw gear (part of the load-setting system), 9—force sensor.

2.2. Energy-Harvesting Proces

Converting mechanical energy into electrical energy was possible thanks to the use of three MFC patches, which were glued on the shaft surface at intervals of 120°. The MFC patches had standard dimensions that are offered by the Smart Materials Company. The dimensions and material constants of the used MFC patches are listed in Table 2.

Table 2. Dimensions and material constants of MFC patches [15,31,32].

Parameter	Symbol	Unit	Value
Length of active piezoelectric area	l_p	mm	85
Length of active and passive area	l_{MFC}	mm	100
Width of piezoelectric area	w_p	mm	14
Thickness of MFC patch	t_{MFC}	mm	0.3
Thickness of the piezoelectric fiber inside the MFC patch	t_{pf}	mm	0.18
Piezoelectric constant of piezoelectric ceramic	d_{31}	C/N	-185×10^{-12}
Dielectric constant of piezoelectric ceramic	ε_{33}	F/m	1.638×10^{-8}
Young modulus of piezoelectric ceramic	Y_p	Pa	54.05×10^{9}

The two-component X-60 adhesive, manufactured by Hottinger Baldwin Messtechnik GmbH, was used to glue the MFC patch on the shaft surface. X-60 adhesive does not contain plasticizers, thanks to which stresses in the glued MFC patch should be equal to the stresses which are in the shaft. Variable stresses in the shaft were generated by the

simultaneous operation of the load-setting system and the rotational-motion-setting system. The load-setting system caused a generation of tensile stress along 1 axis in one side of the shaft and compressive stress along 1 axis in the second side [12]. The values of both stresses decreased in the direction of the shaft symmetry axis (along axis 3), where they reached 0. The values of the stresses on the shaft surface are the highest for such types of shaft bending. The schema of the stress distribution in the shaft is presented in Figure 3.

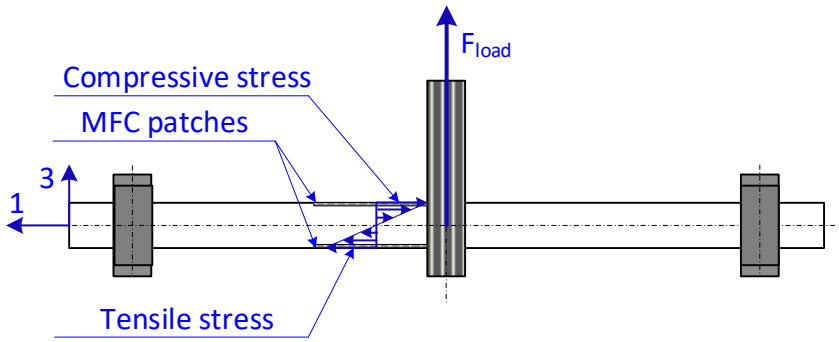

Figure 3. Schema of stress in a loaded shaft.

The rotational-motion-setting system caused a cyclic change in stresses, e.g., a rotation by 180 degrees generated a change in the compressive stresses into tensile and tensile into compressive. The maximum values of both tensile and compressive stress occurred in the place where the belt transmission was mounted to the shaft. Values of both stresses decreased in the direction of the bearings (along axis 1), where they reached 0. Taking into account that the polarization of the piezoelectric fibers in the MFC patch was along 3 axes and both compressive and tensile stress acted along 1 axis, the constitutive equations of the piezoelectric effect are the following [12]:

$$\begin{aligned} S_1 &= s_{11}^E T_1 + d_{31} E_3 \\ D_3 &= d_{31} T_1 + \varepsilon_{33}^T E_3 \end{aligned} \quad (1)$$

where S is the strain, T is the stress, D is the electric induction, E is the electric field intensity, s is the compliance constant at constant electric field, d is the electromechanical coupling constant, and ε is the permeability tensor at constant stress.

2.3. Connection Structures of MFC Patches and Rectifiers

These MFC patches were connected by the use of four circuits, which are presented in Figure 4. These are:

- First: a delta circuit created by three MFC patches and connected with a three-phase rectifier (Figure 4a);
- Second: a star circuit created by three MFC patches and connected with a three-phase rectifier (Figure 4b);
- Third: a parallel connection of three circuits, each of which consists of an MFC patch and a full bridge rectifier (Figure 4c);
- Fourth: a series connection of three circuits, each of which consists of an MFC patch and a full bridge rectifier (Figure 4d).

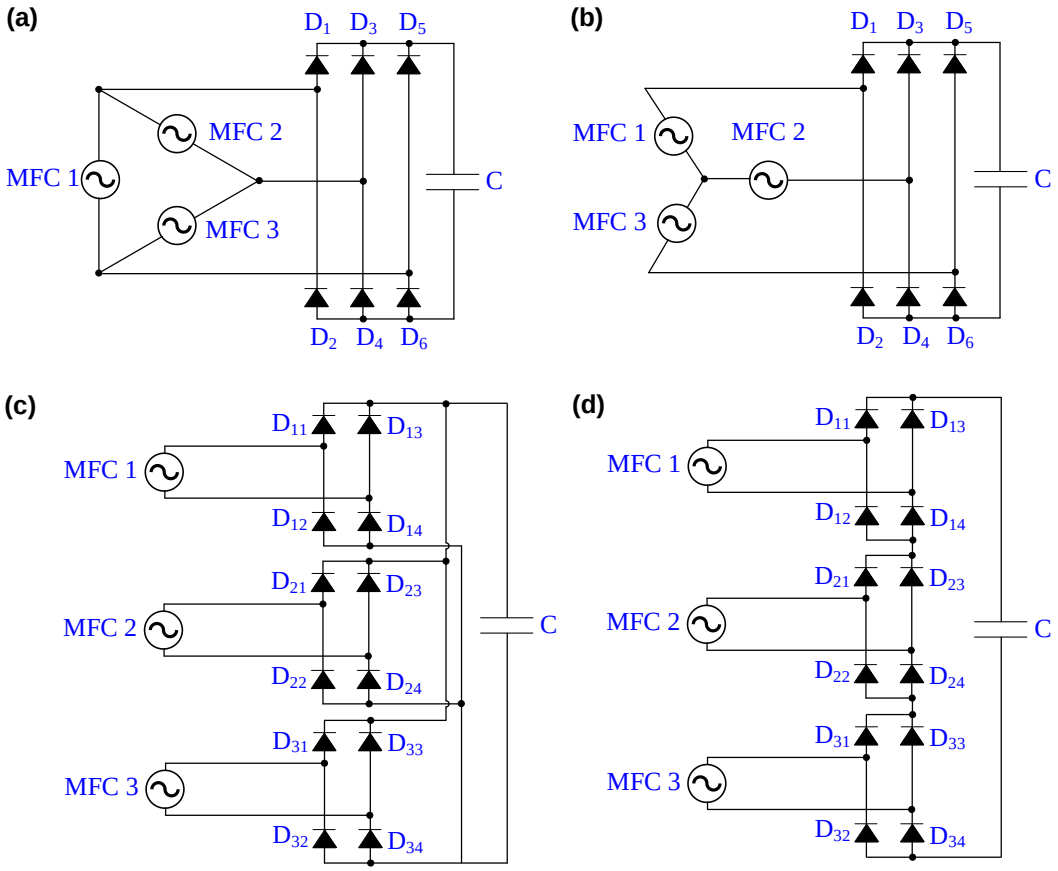

Figure 4. Connection structures of three MFC elements: (**a**) Delta; (**b**) Star; (**c**) Parallel; (**d**) Series.

The rectifiers used in all connection structures contained similar standard silicones diodes. The selection of similar diodes allowed for eliminating the diodes' influence (described, e.g., in [33]) on the energy-harvesting process. For parallel and series connections, the basic full bridge rectifier (SEH) was used to perform a comparative analysis of these connection structures with structures which containing a three-phase rectifier. To the best of the authors' knowledge, there are currently no connection structures with a three-phase rectifier described in the literature that correspond to extended SEH systems, e.g., P-SSHI or S-SSHI.

2.4. Measurement System

The measurement system consisted of an A/D board, a voltage divider, a voltage amplifier, and a force sensor. The A/D Board, which was a DaQBoard 2000 produced by IOTech, Newcastle upon Tyne, UK, had the most important parameters: maximum input voltage equal to $\pm$11 V and maximum sample rate equal to 200 kHz. The voltage divider was used to reduce the measured voltage to a value not exceeding $\pm$10 V. The voltage amplifier, which was an ADAM 3016 produced by Advantech, was used to transform voltage from range of mV to a range of V. The force sensor, which was an L6E sensor produced by the Zemic Europe B.V. company, had the most important parameters: maximum measured force equal to 981 N and combined error $\leq \pm 0.0175\%$.

The slip ring device, manufactured by Hottinger Baldwin Messtechnik HBM, connected the three MFC patches with the energy storage system. Wires, which were among the MFC patches and the slip ring assembly, were led through the inside of the rotating shaft.

2.5. Program of Laboratory Research

The four connection structures mentioned above were tested in 12 laboratory experiments. Table 3 presents the conditions of the experiments.

Table 3. Variable values in each laboratory experiment.

			Number of Experiment											
			1	**2**	**3**	**4**	**5**	**6**	**7**	**8**	**9**	**10**	**11**	**12**
Variable	**Symbol**	**Unit**	**Value**											
Shaft bending force	F_b	N	200	200	200	200	200	200	400	400	400	400	400	400
Rotational speed of shaft	n	rps	10	20	10	20	10	20	10	20	10	20	10	20
Capacity of capacitor	C	μF	250	250	500	500	10^3	10^3	250	250	500	500	10^3	10^3

Each of the four connection structures was tested for 500 s in each experiment from 1 to 12. Hence, the time of each experiment was 2000 s. The measurement was performed at a frequency of 1 KHz. In order to obtain legible graphs, the average of the measurements obtained in individual second was calculated. These averages were used to construct the waveform graphs presented in the next chapter.

3. Results

3.1. Charging Electrical Current and Charging Power of the Capacitor

Figure 5 presents the electrical current generated by the three MFC in the first and second laboratory experiments during charging of the capacitor. Due to the fact that the measurements were made once every second, the courses of charging electrical current are not smooth, with some noise. The maximum values of generated electrical current in all of 12 experiments are presented in Table 4.

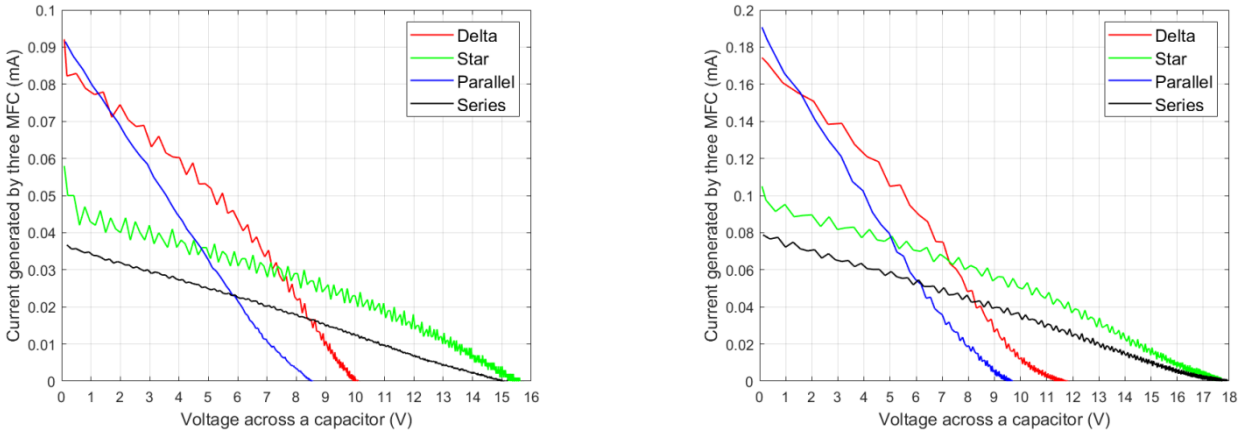

(**a**) (**b**)

Figure 5. Charging electrical current generated for a bending force of 200 N and a capacity of the capacitor of 250 μF: (**a**) rotational speed is 10 rps; (**b**) rotational speed is 20 rps.

Table 4. Maximum values of generated electrical current by the MFC patches.

Connection	**Number of Experiment**											
	1	**2**	**3**	**4**	**5**	**6**	**7**	**8**	**9**	**10**	**11**	**12**
	Maximum Values of Electrical Current (mA)											
Delta	**0.092**	0.174	0.091	0.089	0.089	0.179	0.178	0.350	0.178	0.350	0.176	0.350
Star	0.058	0.105	0.057	0.059	0.059	0.107	0.104	0.200	0.104	0.200	0.104	0.210
Parallel	**0.092**	**0.190**	**0.092**	**0.091**	**0.091**	**0.192**	**0.194**	**0.396**	**0.197**	**0.397**	**0.197**	**0.400**
Series	0.036	0.078	0.036	0.037	0.038	0.082	0.087	0.200	0.088	0.200	0.087	0.210

The charging power of a capacitor (P_C) was calculated by the use of the formula:

$$P_C = \frac{d\left(\frac{1}{2}C_C V_C^2\right)}{dt} \quad (2)$$

where: C_C is a capacitor's capacity and V_C is the voltage across a capacitor.

Figure 6 presents the capacitor charging power in the first and second laboratory experiments during charging of the capacitor. The maximum values of the capacitor charging power in all of the 12 experiments are presented in Table 5.

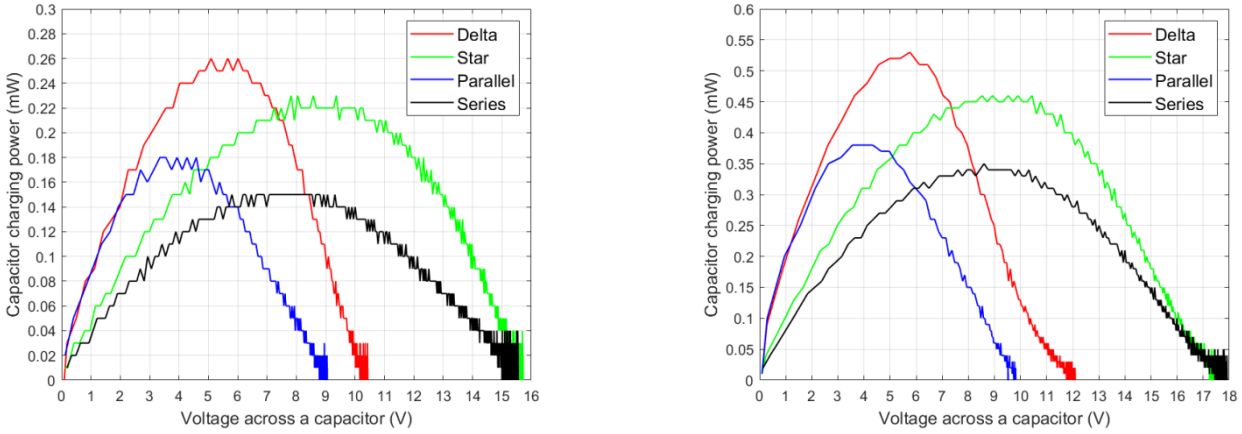

Figure 6. Capacitor charging power for a bending force of 200 N and a capacity of the capacitor of 250 µF: (**a**) rotational speed is 10 rps; (**b**) rotational speed is 20 rps.

Table 5. Maximum values of the capacitor charging power.

Connection	Number of Experiment											
	1	**2**	**3**	**4**	**5**	**6**	**7**	**8**	**9**	**10**	**11**	**12**
	Maximum Values of Capacitor Charging Power (mW)											
Delta	**0.26**	**0.53**	**0.26**	**0.52**	**0.27**	**0.54**	**0.90**	**1.87**	**0.91**	**1.83**	**0.90**	**1.89**
Star	0.23	0.46	0.23	0.50	0.24	0.48	0.81	1.72	0.81	1.67	0.78	1.69
Parallel	0.18	0.38	0.18	0.38	0.18	0.38	0.70	1.42	0.68	1.40	0.68	1.43
Series	0.15	0.35	0.16	0.33	0.19	0.34	0.57	1.40	0.57	1.30	0.57	1.30

3.2. Voltage across a Capacitor and Energy Stored in Capacitor

Figure 7 presents the voltage across a capacitor during the charging process in the first and second laboratory experiments. The maximum values of voltage across a capacitor in all of the 12 experiments are presented in Table 6.

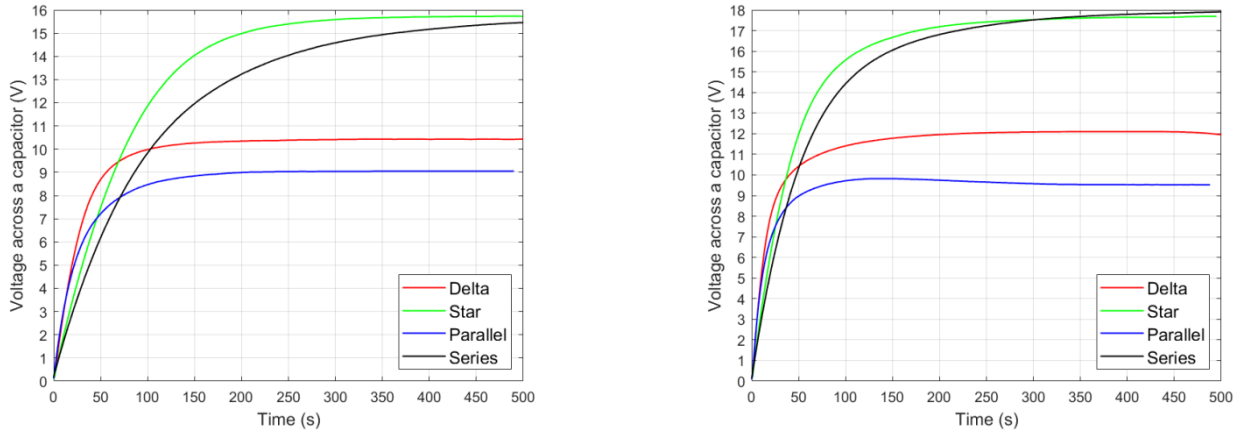

Figure 7. Voltage across a capacitor for a bending force of 200 N and a capacity of the capacitor of 250 µF: (**a**) rotational speed is 10 rps; (**b**) rotational speed is 20 rps.

Table 6. Maximum voltage across a capacitor.

Connection	Number of Experiment											
	1	**2**	**3**	**4**	**5**	**6**	**7**	**8**	**9**	**10**	**11**	**12**
	Maximum Values of Voltage (V)											
Delta	10.43	12.10	10.42	12.00	10.12	11.54	19.80	18.30	19.52	18.34	17.12	18.15
Star	**15.72**	**17.69**	**15.10**	**17.52**	**12.48**	**15.95**	28.02	**29.51**	**27.61**	**29.06**	**23.59**	**27.11**
Parallel	9.05	9.82	9.07	10.32	8.68	9.75	17.18	17.77	17.10	17.75	16.30	17.66
Series	15.33	17.85	13.68	16.85	10.59	14.61	**29.02**	28.00	25.96	28.00	20.27	26.00

Energy stored in the capacitor (E_C) was calculated by the use of the formula:

$$E_C = \frac{1}{2} C_C V_C^2 \tag{3}$$

Table 7 presents energy stored in the capacitor in all of the 12 experiments. Energy stored in the capacitor in the first, third, and fifth laboratory experiments are presented in Figure 8.

Table 7. Maximum energy stored in a capacitor in a time range from 0 to 500 s.

Connection	Number of Experiment											
	1	**2**	**3**	**4**	**5**	**6**	**7**	**8**	**9**	**10**	**11**	**12**
	Maximum Energy Stored in Capacitor (mJ)											
Delta	13.6	18.3	27.1	36.0	51.2	66.5	49.0	41.8	95.2	84.1	146.5	164.7
Star	**30.9**	39.1	**58.3**	**77.3**	**85.5**	**132.1**	98.1	**108.9**	**191.1**	**211.1**	**281.6**	**367.4**
Parallel	10.2	12.0	20.5	26.6	37.6	47.5	36.8	39.4	73.1	78.8	132.8	156.1
Series	29.8	**40.1**	49.4	73.1	63.4	113.6	**106.4**	98.0	177.8	98.0	227.4	84.5

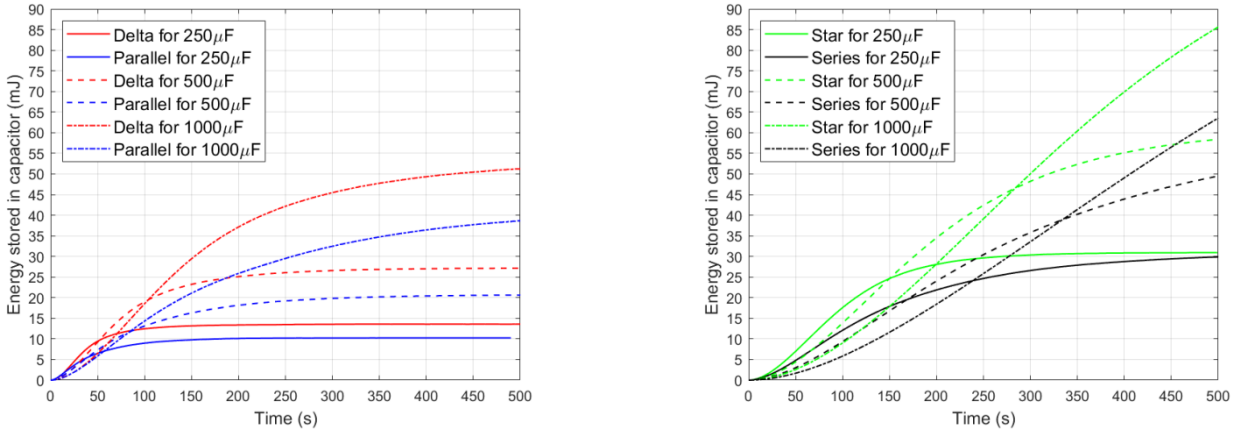

(**a**) (**b**)

Figure 8. Energy stored in the capacitor for a bending force of 200 N and a rotational speed of 10 rps: (**a**) comparison of the delta and parallel connections; (**b**) comparison of the star and series connections.

4. Discussion

The maximum values of the capacitor-charging electrical current were generated by three MFC patches which were connected in parallel (Figure 5). The maximum electrical current values were generated by this connection regardless of changes in the capacitance of the capacitor, the force loading the shaft, or the speed of rotation of the shaft. However, there are two points to note: (1) the capacitor-charging electrical current generated by the parallel connection decreased sharply with increasing voltage across the capacitor, and (2) the parallel connection generated the highest value of charging electrical current only

for low levels of voltage across the capacitor (up to 1–2 V). To explain the generation of the highest charging electrical current by the parallel connection for low voltage levels on the capacitor, the known rules need to be considered: (1) In a parallel connection, the currents add up. Hence, the average charging electrical current for the parallel connection of three full bridge rectifiers is:

$$i_{parallel} = \frac{2}{\pi} i_{pmax1} + \frac{2}{\pi} i_{pmax2} + \frac{2}{\pi} i_{pmax3} \quad (4)$$

where i_{pmaxn} is an amplitude of the current generated by the MFC patch no n (assuming that $i_{pmax1} = i_{pmax2} = i_{pmax3} = i_{pmaxn}$ received $i_{parallel} = 1.91 i_{pmaxn}$). (2) In a delta connection, the average current is calculated as:

$$i_{delta} = \sqrt{3} i_{pmaxn} \approx 1.73 i_{pmaxn} \quad (5)$$

As can be seen, the average charging current generated by a parallel connection should theoretically be around 10% larger than that generated by a delta connection. Based on the data from the 12 experiments presented in Table 4, it was calculated that the maximum charging current generated by the parallel connection was, on average, 10.14% larger compared to the current generated by the delta connection.

In order to compare the charging electrical currents at higher levels of voltage across a capacitor, the average charging electrical current was calculated over the entire duration of each experiment. The average of the generated electrical current in 500 s in all 12 experiments is presented in Table 8.

Table 8. Average of generated electrical current by MFC patches.

Connection	Number of Experiment											
	1	**2**	**3**	**4**	**5**	**6**	**7**	**8**	**9**	**10**	**11**	**12**
	Average Values of Electrical Current (μA)											
Delta	3.1	4.7	8.7	11.1	20.1	23.9	13.4	14.5	24.1	24.5	46.2	47.5
Star	**7.3**	**11.0**	**15.4**	**19.4**	**26.4**	**37.7**	**20.4**	**29.9**	**35.5**	**50.0**	**58.5**	**86.2**
Parallel	1.7	2.8	7.0	8.7	16.2	19.1	9.5	11.5	19.5	24.9	38.0	44.7
Series	6.5	9.2	12.9	18.3	21.7	32.8	**20.4**	**28.0**	33.0	**48.0**	47.8	**84.0**

The first observation is that the highest average values of the charging electrical current were generated by the star circuit, regardless of the value of the capacitor capacity, the external load of the shaft, or its rotational speed. To explain the generation of the highest average charging electrical current by the star connection, the known rules need to be considered: (1) the capacitor is charged when the voltage generated by the MFC patches is larger than the voltage across the capacitor, and it is discharged when the voltage generated is lower than the voltage across the capacitor [34,35]; (2) in the parallel and delta connections the output voltage is approximately equal to the voltage generated by one MFC patch (assuming that all MFC patches generate the same voltage values); (3) in a series connection, the voltages add up; and (4) in a star connection, the average current is calculated as:

$$u_{star} = \sqrt{3} u_{pmaxn} \approx 1.73 u_{pmaxn} \quad (6)$$

where u_{maxn} is an amplitude of the current generated by MFC patch no n.

Parallel and delta connections generate lower voltages than series and star connections, so the larger the voltage across the capacitor, the more frequently there are discharge times for the capacitor. The series and star connections generate higher voltages, so there will be a lower sum of discharge times for the capacitor. It should also be noted that the use of a three-phase rectifier in the star connection causes the output voltage in this connection to show less instantaneous drops compared to the series connection. The star connection generated the greater values of average charging electrical current in comparison to the

rest of connections, appropriately greater by 9.68% compared to the series connection, greater by 64.47% compared to the delta connection, and greater by 95.33% compared to the parallel connection. As a result, the star circuit made it possible to obtain the highest values of voltage across a capacitor in the long time (Figure 9).

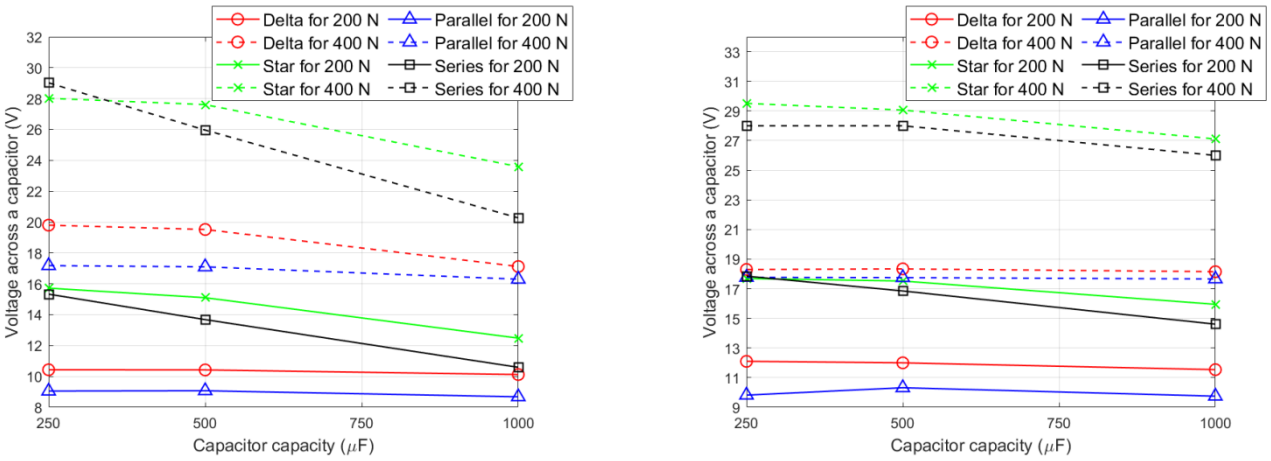

Figure 9. Maximum voltage across a capacitor for a charging period equal to 500 s: (**a**) rotational speed is 10 rps; (**b**) rotational speed is 20 rps.

An analysis of the capacitor-charging dynamics for individual connections indicates that the delta connection produced the highest capacitor-charging power, regardless of the value of the capacitor capacity, the external load of the shaft, or its rotational speed (Figure 10).

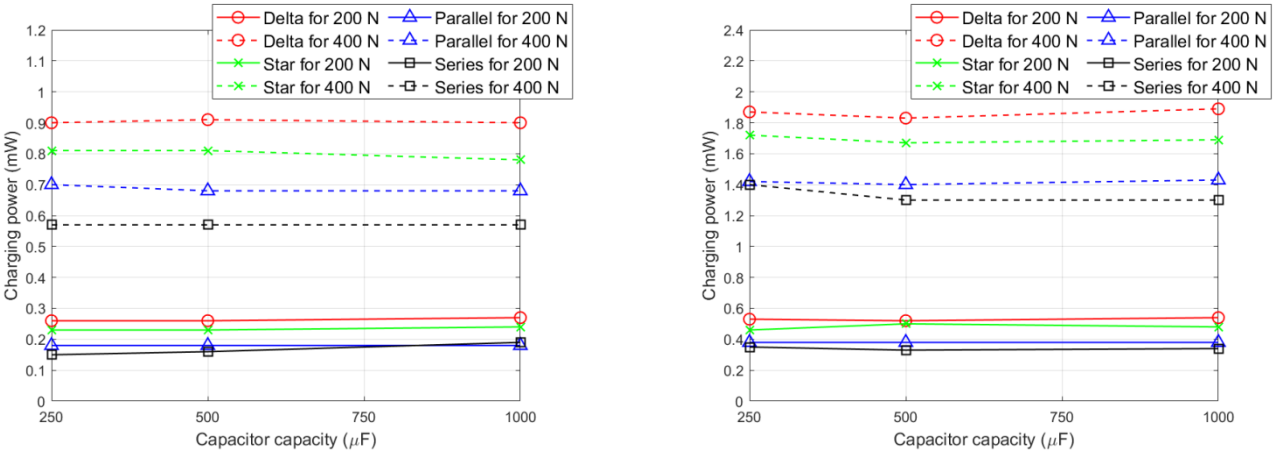

Figure 10. Maximum charging power: (**a**) rotational speed is 10 rps; (**b**) rotational speed is 20 rps.

Many researchers use the commercial EH300 or EH301 energy storage systems, in which the voltage across the capacitor reaches a maximum value of 3.6 V [36] or 5.2 V [37]. Tables 9 and 10 show the times to reach 3.6 V and 5.2 V across a capacitor in all 12 experiments.

Table 9. Time to reach 3.6 V across a capacitor.

Connection	Number of Experiment											
	1	**2**	**3**	**4**	**5**	**6**	**7**	**8**	**9**	**10**	**11**	**12**
	Time (s)											
Delta	**13**	**7**	**26**	**13**	**50**	**26**	7	**4**	16	**7**	24	**12**
Star	21	11	42	21	83	41	10	6	21	10	40	20
Parallel	14	8	27	14	54	27	**6**	**4**	**12**	9	**22**	**12**
Series	26	13	53	26	107	51	13	6	23	10	45	20

Table 10. Time to reach 5.2 V across a capacitor.

Connection	Number of Experiment											
	1	**2**	**3**	**4**	**5**	**6**	**7**	**8**	**9**	**10**	**11**	**12**
	Time (s)											
Delta	**20**	**11**	**41**	**20**	**80**	**41**	10	6	22	**10**	36	**18**
Star	32	17	64	32	127	62	15	8	31	15	59	30
Parallel	24	12	47	23	95	46	**9**	**5**	**19**	12	**35**	**18**
Series	40	20	82	41	165	79	19	8	35	15	69	30

Based on the data in Tables 9 and 10, it can be seen that the parallel connection always allows a shorter capacitor-charging time compared to the series connection for the analyzed voltage levels across the capacitor. This observation agrees with the results of other researchers who compared the parallel and serial connections of two MFC patches glued to a cantilever beam, e.g., Yang et al. [38] noticed that a parallel connection is the most efficient to charge a capacitor for a voltage across the capacitor from 1.8 to 3.6 V. However, what is new is the observation that the shortest times to reach a voltage on the capacitor equal to 3.6 V and 5.2 V were achieved more often by the delta connection than by the parallel. The delta connection always generated voltage equal to 3.6 V or 5.2 V across a capacitor in the shortest time for a lower level of load-force value (200 N). The delta connection generated a target voltage equal to 3.6 V and 5.2 V across a capacitor in an average time shorter, respectively, by 6.25% and 13.76% compared to the parallel connection. For a higher level of load-force value (400 N), the delta and parallel connections generated voltages across a capacitor equal to 3.6 V or 5.2 V in more comparable times. However, the delta connection generated target voltages equal to 3.6 V and 5.2 V across a capacitor in an average time shorter, respectively, by 7.14% and 3.92% compared to the delta connection for a level of stress in the shaft caused by a bending force of 400 N.

5. Conclusions

Energy collection in a capacitor, which was charged by four connection structures of MFC patches, was the subject of laboratory research. The first structure was the delta circuit created by three MFC patches and connected with three-phase rectifier; the second structure was the delta circuit created by three MFC patches and connected with three-phase rectifier; the third structure was the parallel connection of three circuits, each of which consisted of an MFC patch and a full bridge rectifier; and the fourth structure was the series connection of three circuits, each of which consisted of an MFC patch and a full bridge rectifier.

The star connection generated the highest values of average charging electrical current, and the other connections can be ranked according to the decrease in the average value of the generated charging electrical current in the following way: series, delta, and parallel. The star connection generated an average charging current greater by 9.68% compared to the series connection, greater by 64.47% compared to the delta connection, and greater by 95.33% compared to the parallel connection. As a result, the star connection makes it possible to obtain the highest values of voltage across a capacitor in the long time period. However, the delta connection produced the highest capacitor-charging power and the

other connections can be ranked according to the decrease in the average value of the generated capacitor-charging power in the following way: star, parallel, and series. The delta connection generated an average charging current greater by 11% compared to the star connection, greater by 33.66% compared to the parallel connection, and greater by 47.71% compared to the series connection.

The shortest time to reach voltages across a capacitor equal to 3.6 V and 5.2 V, which are the standard values for commercial EH300 or EH301 energy storage systems, is achieved by use of both the delta and parallel connection. The choice of one of these connections depends on the load conditions of the shaft. The delta connection generated target voltages equal to 3.6 V and 5.2 V across a capacitor in an average time shorter, respectively, by 6.25% and 13.76% compared to the parallel connection for a level of stress in the shaft caused by a bending force 200 N. For target voltages across a capacitor equal to 3.6 V and 5.2 V, the difference between the charging times by the delta circuit and by the parallel connection decreased as the stress in the shaft increased, and, finally, the parallel connection generated a shorter loading time. The delta connection generated target voltages equal to 3.6 V and 5.2 V across a capacitor in average times shorter, respectively, by 7.14% and 3.92% compared to the delta connection for a level of stress in the shaft caused by a bending force 400 N.

The article proves that, in the process of charging a capacitor by MFC patches, the energy accumulated in this capacitor depends not only on the changes in stresses in the piezoelectric ceramics (which is known from the literature), but also on two interrelated factors: the connection structure of the MFC patches and the level of voltage across the capacitor. Such results for delta and star connections have not been previously reported in the literature. The presented conclusions from the research can be used to choose an MFC patch connection structure for the selected value of the target voltage level on the capacitor.

Author Contributions: Conceptualization, P.M. and D.G.; methodology, P.M. and D.G.; investigation, P.M. and D.G.; writing—original draft preparation, D.G.; writing—review and editing, D.G.; supervision, D.G. All authors have read and agreed to the published version of the manuscript.

Funding: This research was funded by the AGH University of Science and Technology within the scope of research program No. 16.16.130.942 and the Initiative for Excellence-Research University at AGH UST.

Institutional Review Board Statement: Not applicable.

Informed Consent Statement: Not applicable.

Data Availability Statement: Data is contained within the article.

Conflicts of Interest: The authors declare no conflict of interest.

References

1. Zhang, J.; Fang, Z.; Shu, C.; Zhang, J.; Zhang, Q.; Li, C. A rotational piezoelectric energy harvester for efficient wind energy harvesting. *Sens. Actuators A Phys.* **2017**, *262*, 123–129. [CrossRef]
2. Rui, X.; Zeng, Z.; Zhang, Y.; Li, Y.; Feng, H.; Huang, X.; Sha, Z. Design and experimental investigation of a self-tuning piezo-electric energy harvesting system for intelligent vehicle wheels. *IEEE Trans. Veh. Technol.* **2019**, *69*, 1440–1451. [CrossRef]
3. Machado, S.P.; Febbo, M.; Ramírez, J.M.; Gatti, C.D. Rotational double-beam piezoelectric energy harvester impacting against a stop. *J. Sound Vib.* **2020**, *469*, 115141. [CrossRef]
4. Khazaee, M.; Rezaniakolaie, A.; Moosavian, A.; Rosendahl, L. A novel method for autonomous remote condition monitoring of rotating machines using piezoelectric energy harvesting approach. *Sens. Actuators A Phys.* **2019**, *295*, 37–50. [CrossRef]
5. Wang, Z.; He, L.; Gu, X.; Yang, S.; Wang, S.; Wang, P.; Cheng, G. Rotational energy harvesting systems using piezoelectric materials: A review. *Rev. Sci. Instrum.* **2021**, *92*, 041501. [CrossRef]
6. Raja, V.; Umapathy, M.; Uma, G.; Kumar, B.P.; Premkumar, S. Design, analysis and experimental investigation of a rotational piezoelectric energy harvester with storage system. *J. Mech. Sci. Technol.* **2020**, *34*, 4475–4487. [CrossRef]
7. Wang, S.; Yang, Z.; Kan, J.; Chen, S.; Chai, C.; Zhang, Z. Design and characterization of an amplitude-limiting rotational piezoelectric energy harvester excited by a radially dragged magnetic force. *Renew. Energy* **2021**, *177*, 1382–1393. [CrossRef]
8. Guan, M.; Liao, W.-H. Design and analysis of a piezoelectric energy harvester for rotational motion system. *Energy Convers. Manag.* **2016**, *111*, 239–244. [CrossRef]

9. Wu, W.-H.; Kuo, K.-C.; Lin, Y.-H.; Tsai, Y.-C. Non-contact magnetic cantilever-type piezoelectric energy harvester for rotational mechanism. *Microelectron. Eng.* **2018**, *191*, 16–19. [CrossRef]
10. Chilabi, H.J.; Salleh, H.; Al-Ashtari, W.; Supeni, E.E.; Abdullah, L.C.; As'Arry, A.B.; Rezali, K.A.M.; Azwan, M.K. Rotational piezoelectric energy harvesting: A comprehensive review on excitation elements, designs, and performances. *Energies* **2021**, *14*, 3098. [CrossRef]
11. Wang, J.-X.; Su, W.-B.; Li, J.-C.; Wang, C.-M. A rotational piezoelectric energy harvester based on trapezoid beam: Simulation and experiment. *Renew. Energy* **2022**, *184*, 619–626. [CrossRef]
12. Grzybek, D.; Micek, P. Piezoelectric energy harvesting based on macro fiber composite from a rotating shaft. *Phys. Scr.* **2019**, *94*, 095802. [CrossRef]
13. Koszewnik, A.; Ołdziej, D.; Amaro, M.B. Parameter optimization of a magnetic coupled piezoelectric energy harvester with the homogenized material—numerical approach and experimental study. *Sensors* **2022**, *22*, 4073. [CrossRef]
14. Roundy, S.; Tola, J. Energy harvester for rotating environments using offset pendulum and nonlinear dynamics. *Smart Mater. Struct.* **2014**, *23*, 105004. [CrossRef]
15. Micek, P.; Grzybek, D. Experimental analysis of the arrays of macro fiber composite patches for rotational piezoelectric energy harvesting from a shaft. *Energies* **2021**, *14*, 4815. [CrossRef]
16. Zhao, L.-C.; Zou, H.-X.; Yan, G.; Liu, F.-R.; Tan, T.; Wei, K.-X.; Zhang, W.-M. Magnetic coupling and flex tensional amplification mechanisms for high-robustness ambient wind energy harvesting. *Energy Convers. Manag.* **2019**, *201*, 112166. [CrossRef]
17. Na, Y.; Lee, M.-S.; Lee, J.W.; Jeong, Y.H. Wind energy harvesting from a magnetically coupled piezoelectric bimorph cantilever array based on a dynamic magneto-piezo-elastic structure. *Appl. Energy* **2020**, *264*, 114710. [CrossRef]
18. Ramezanpour, R.; Nahvi, H.; Ziaei-Rad, S. A vibration-based energy harvester suitable for low-frequency, high-amplitude environments: Theoretical and experimental investigations. *J. Intell. Mater. Syst. Struct.* **2015**, *27*, 642–665. [CrossRef]
19. Fang, S.; Fu, X.; Du, X.; Liao, W.-H. A music-box-like extended rotational plucking energy harvester with multiple piezoelectric cantilevers. *Appl. Phys. Lett.* **2019**, *114*, 233902. [CrossRef]
20. Yang, Y.; Shen, Q.; Jin, J.; Wang, Y.; Qian, W.; Yuan, D. Rotational piezoelectric wind energy harvesting using impact-induced resonance. *Appl. Phys. Lett.* **2014**, *105*, 053901. [CrossRef]
21. Kim, G.W. Piezoelectric energy harvesting from torsional vibration in internal combustion engines. *Int. J. Automot. Technol.* **2015**, *16*, 645–651. [CrossRef]
22. Yan, L.; Hou, J.; Yang, Z.; Chu, X. Design and experimental characterization of a vibration energy harvesting device for rotational systems. *Adv. Mech. Eng.* **2013**, *5*, 263614. [CrossRef]
23. Cheng, C.; Chen, Z.; Xiong, Y.; Shi, H.; Yang, Y. A high-efficiency, self-powered nonlinear interface circuit for bi-stable rotating piezoelectric vibration energy harvesting with nonlinear magnetic force. *Int. J. Appl. Electromagn. Mech.* **2016**, *51*, 235–248. [CrossRef]
24. Bai, F.; Song, G.; Dong, W.; Guan, L.; Bao, H. Fan-structure wind energy harvester using circular array of polyvinylidene fluoride cantilevers. *J. Intell. Mater. Syst. Struct.* **2016**, *28*, 653–662. [CrossRef]
25. Yang, B.; Yi, Z.; Tang, G.; Liu, J. A gullwing-structured piezoelectric rotational energy harvester for low frequency energy scavenging. *Appl. Phys. Lett.* **2019**, *115*, 063901. [CrossRef]
26. Kurt, E.; Cottone, F.; Uzun, Y.; Orfei, F.; Mattarelli, M.; Özhan, D. Design and implementation of a new contactless triple piezoelectrics wind energy harvester. *Int. J. Hydrog. Energy* **2017**, *42*, 17813–17822. [CrossRef]
27. Bouzelata, Y.; Kurt, E.; Uzun, Y.; Chenni, R. Mitigation of high harmonicity and design of a battery charger for a new piezo-electric wind energy harvester. *Sens. Actuators A Phys.* **2018**, *273*, 72–83. [CrossRef]
28. Pajchrowski, T.; Krystkowiak, M.; Matecki, D. Modulation variants in DC circuits of power rectifier systems with improved quality of energy conversion—Part I. *Energies* **2021**, *14*, 1876. [CrossRef]
29. Bagheri, S.; Wu, N.; Filizadeh, S. Modeling of capacitor charging dynamics in an energy harvesting system considering accurate electromechanical coupling effects. *Smart Mater. Struct.* **2018**, *27*, 065026. [CrossRef]
30. Zhang, Z.; Xiang, H.; Tang, L. Modeling, analysis and comparison of four charging interface circuits for piezoelectric energy harvesting. *Mech. Syst. Signal Process.* **2021**, *152*, 107476. [CrossRef]
31. Smart Material—Home of the MFC. Available online: https://www.smart-material.com/MFC-product-mainV2.html (accessed on 15 April 2022).
32. Deraemaeker, A.; Nasser, H.; Benjeddou, A.; Preumont, A. Mixing rules for the piezoelectric properties of macro fiber composites. *J. Intell. Mater. Syst. Struct.* **2009**, *20*, 1475–1482. [CrossRef]
33. Yuan, M.; Cao, Z.; Luo, J. Characterization the influences of diodes to piezoelectric energy harvester. *Int. J. Smart Nano Mater.* **2018**, *9*, 151–166. [CrossRef]
34. Prasath, S.S.; Arockiarajan, A. Influence of bonding layer on effective electromechanical properties of macro-fiber composites (MFCs). *Smart Mater. Struct.* **2014**, *23*, 095046. [CrossRef]
35. Grzybek, D.; Micek, P. Impact of series and parallel connection of macro fiber composite patches in piezoelectric harvester on energy storage. *Energies* **2021**, *14*, 2379. [CrossRef]
36. Peigney, M.; Siegert, D. Piezoelectric energy harvesting from traffic-induced bridge vibrations. *Smart Mater. Struct.* **2013**, *22*, 095019. [CrossRef]

37. Mystkowski, A.; Ostasevicius, V. Experimental study of macro fiber composite-magnet energy harvester for self-powered active magnetic bearing rotor vibration sensor. *Energies* **2020**, *13*, 4806. [CrossRef]
38. Yang, Y.; Tang, L.; Li, H. Vibration energy harvesting using macro-fiber composites. *Smart Mater. Struct.* **2009**, *18*, 115025. [CrossRef]